Applied Physics Letters ARTICLE scitation.org/journal/apl

Stress-tuning the bulk photovoltaic response in polycrystalline bismuth ferrite films

Cite as: Appl. Phys. Lett. **122**, 152903 (2023); doi: 10.1063/5.0136800
Submitted: 29 November 2022 · Accepted: 22 March 2023 ·
Published Online: 11 April 2023

View Online Export Citation CrossMark

Alfredo Blázquez Martínez,[1,2,3,a)] Patrick Grysan,[1] Stéphanie Girod,[1] Veronika Kovacova,[1,3] Sebastjan Glinsek,[1,3] and Torsten Granzow[1,3]

AFFILIATIONS

[1]Luxembourg Institute of Science and Technology, Materials Research and Technology Department, 41 rue du Brill, Belvaux L-4422, Luxembourg
[2]University of Luxembourg, 41 rue du Brill, Belvaux L-4422, Luxembourg
[3]Inter-institutional Research Group Uni.lu–LIST on Ferroic Materials, 41 rue du Brill, Belvaux L-4422, Luxembourg

[a)]Author to whom correspondence should be addressed: alfredo.blazquez@list.lu

ABSTRACT

Bulk or anomalous photovoltaic effect in ferroelectrics has recently sparked interest due to the generation of switchable photovoltages that are not limited by the bandgap of the material. The development of strategies to tune its magnitude is a key for the development of light-driven devices, e.g., photostrictive actuators, photostrictive sensors, or reconfigurable waveguides. In this paper, the bulk photovoltaic effect of polycrystalline solution-deposited bismuth ferrite thin films is studied under different stress conditions induced by different substrates and quantified using a direct strain assessment via x-ray diffraction. An increase in the short-circuit bulk photovoltaic current of 150% is observed with a change from a compressive stress of 0.54 GPa to a tensile stress of 0.93 GPa. This change is attributed to intrinsic piezophotovoltaic effect, demonstrating the potential to strain engineer the bulk photovoltaic effect in thin films.

Bulk or anomalous photovoltaic (BPV) effect in ferroelectric materials consists of the generation of photovoltage in a material under homogeneous illumination.[1] This effect, different from traditional interface-based photovoltaics, allows for the generation of above-bandgap photovoltages,[2,3] which are interesting for the nondestructive readout mechanism for optical memories,[4] applications related to photorefractive,[5–7] or photostrictive[8,9] devices. The BPV effect has received renewed interest in recent decades due to the possibility of obtaining power conversion efficiencies higher than the Shockley–Queisser limit.[1,3] Several strategies have been used to engineer the BPV effect and boost the photovoltaic response; the modulation of the domain structure,[10–12] the reduction in the bandgap by cation substitution,[13] defect engineering,[14,15] and the use of tip-enhanced methods[3,16] have been discussed as ways to tune the photovoltaic response in ferroelectrics. The BPV effect has only been traditionally explored in single crystals or epitaxial thin films; only very recently, a true proof of a BPV charge transport was evidenced in a polycrystalline film.[17]

Between the different strategies, strain engineering has arisen as a powerful approach to modulate the BPV effect. For example, Yang *et al.* demonstrated that the application of a strain gradient to a centrosymmetric material leads to the appearance of a BPV-like effect they referred to as flexo-photovoltaic effect.[18] Nadupalli *et al.* have recently shown that the BPV effect of $LiNbO_3$ single crystals can be enhanced by the application of a uniaxial compressive strain, referred to as piezophotovoltaic effect.[19] However, this topic remains largely unexplored, and the examples that can be found in the literature are limited to epitaxial films or single crystals. So far, there is no direct observation of an intrinsic piezophotovoltaic effect in ferroelectric thin films.

In this Letter, the BPV effect of polycrystalline solution-processed bismuth ferrite thin films under different levels of strain is studied. The thermal expansion coefficient (TEC) mismatch between the film and the substrate generates strained films. Using substrates with different thermal expansion coefficients, films under in-plane compressive or tensile strain are prepared.[20,21] The magnitude of the BPV effect is shown to increase with increasing in-plane tensile strain. These results constitute evidence of a true intrinsic piezophotovoltaic effect[19,22] in thin films.

Polycrystalline 5% manganese and 2% titanium-doped $BiFeO_3$ films (BFO) were deposited by solution methods following a nitrate-based route. Films were deposited on three different substrates: fused

silica, c-cut sapphire (both Siegert Wafer, Germany), and MgO (Biotain Crystal, China). Assuming a linear thermal expansion coefficient (TEC) of $11.3 \times 10^{-6}\ K^{-1}$ for BFO,[23] both the TECs of fused silica at $0.5 \times 10^{-6}\ K^{-1}$ and of c-cut sapphire at $7 \times 10^{-6}\ K^{-1}$ are lower and, thus, should put the films under tensile residual stress, while MgO with a higher TEC of $13 \times 10^{-6}\ K^{-1}$ should create compressive stress in the films. A detailed description of the film deposition process as well as the influence of processing parameters on the ferroelectric properties and dark conductivity of the BFO films is presented in Ref. 24. A 23 nm thick HfO_2 film was prepared by atomic layer deposition on all substrates as a barrier layer. $(100)_{pc}$ texture was induced to the BFO film using a 16 nm thick $PbTiO_3$ seed layer. The BFO films were crystallized after deposition of each 25 nm thick single layer. Films with a thickness of 200 ± 10 nm were prepared by successive deposition and crystallization. Interdigitated electrodes (IDEs) were used to measure the electrical and photovoltaic properties. Conventional liftoff photolithography and platinum sputtering were used to pattern the IDEs on top of the film. The IDEs consist of 50 pairs of fingers with an effective length of 370 μm. The width of the fingers is 4.5 ± 0.5 μm, and the space between fingers is 2.5 ± 0.5 μm. A more detailed description of the device preparation can be found in a previous report.[17]

The crystal structure was analyzed by x-ray diffraction (XRD) in the θ–2θ configuration on a Bruker D8 diffractometer (Bruker, USA) using Cu-K_α radiation. To quantify the in-plane strain in the films, a direct strain assessment via $\sin^2(\Psi)$ x-ray diffraction was performed. The method is described in detail, e.g., in Refs. 25–27 and the references therein. Atomic force microscopy (AFM) images were obtained in the tapping mode configuration on an MFP-3D infinity (Asylum Research, USA) with an AC160TS-R3 tip (Olympus, Japan). The topography was imaged recording the correspondent Z piezo displacement while maintaining the amplitude of the cantilever's first eigenmode (c. 265 KHz) constant at 70 nm. Piezoforce microscopy (PFM) measurements were conducted on an MFP-3D infinity AFM (Asylum Research, USA) at the contact resonance in the dual amplitude resonance tracking (DART) mode. A 5 kHz and 1 V amplitude sine wave signal was applied to the conductive tip, creating two side bands around the contact resonance. The lock-in demodulation of the lowest frequency sideband was used to record the PFM amplitude and phase responses. The tip used was a conductive single crystal diamond AD-2.8-AS (ADAMA, Ireland) with a typical cantilever stiffness of 2 N/m and a resonance of 75 kHz. The contact resonance is found around 300 kHz.

Polarization hysteresis loops were measured on a TF analyzer 2000 (aixACCT, Germany) at room temperature and at a frequency of 5 kHz. The photovoltaic characterization was performed by measuring the short-circuit current density (J_{SC}) as a function of the time or current density (J) as a function of voltage (V) on a source-meter unit (Keysight, model B2901A). Poling was performed as described in our previous report.[17] The devices were illuminated with a 455 nm LED (Thorlabs, model M455L4 series) with a light intensity of $0.48\ W\ cm^{-2}$. A detailed analysis of the measurement conditions can be found in a previous report.[17]

The XRD patterns of BFO films deposited on fused silica (BFO/FS), sapphire (BFO/Sap), and MgO (BFO/MgO) substrates are shown in Fig. 1(a). The patterns were indexed following the pseudocubic notation. They indicate polycrystalline BFO films with no secondary phases, in agreement with the PDF card of $BiFeO_3$ (#00-066-0439).[28] All the films have an out-of-plane $[100]_{pc}$ texture. A Lotgering factor of 0.65, 0.85, and 0.75 is obtained for BFO/FS, BFO/Sap, and BFO/MgO, respectively. Figures 1(b)–1(d) show the AFM topography images of BFO films deposited on fused silica, sapphire, and magnesium oxide, respectively. All films show a granular microstructure with a grain diameter of 46 ± 15, 46 ± 16, and 55 ± 16 nm for BFO/FS, BFO/Sap, and BFO/MgO, respectively. They show similar roughness of 6 ± 1, 8 ± 2, and 9 ± 3 nm for BFO/FS, BFO/Sap, and BFO/MgO, respectively.

The XRD patterns around the $(110)_{pc}$ peak were recorded under different tilt angles Ψ as shown in Figs. 2(a)–2(c). Using the $d_{(110)}$ spacing for different tilt angles, the in-plane deformation can be extracted from the following relation:

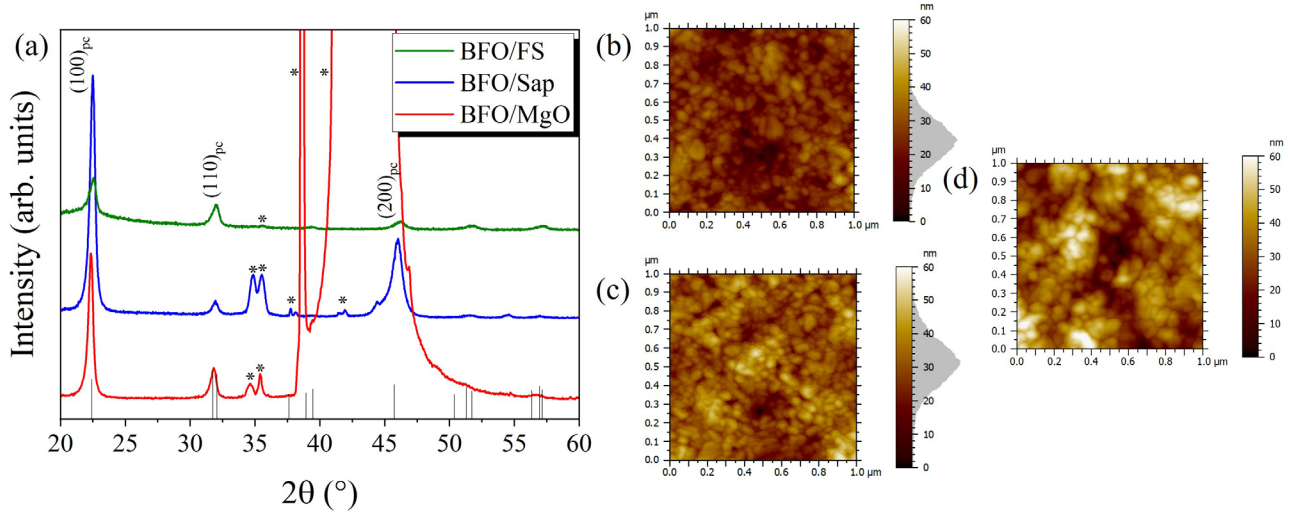

FIG. 1. (a) X-ray pattern of the BFO film on different substrates. * indicates the substrate peaks. AFM topography images of the films deposited on (b) fused silica, (c) sapphire, and (d) magnesium oxide.

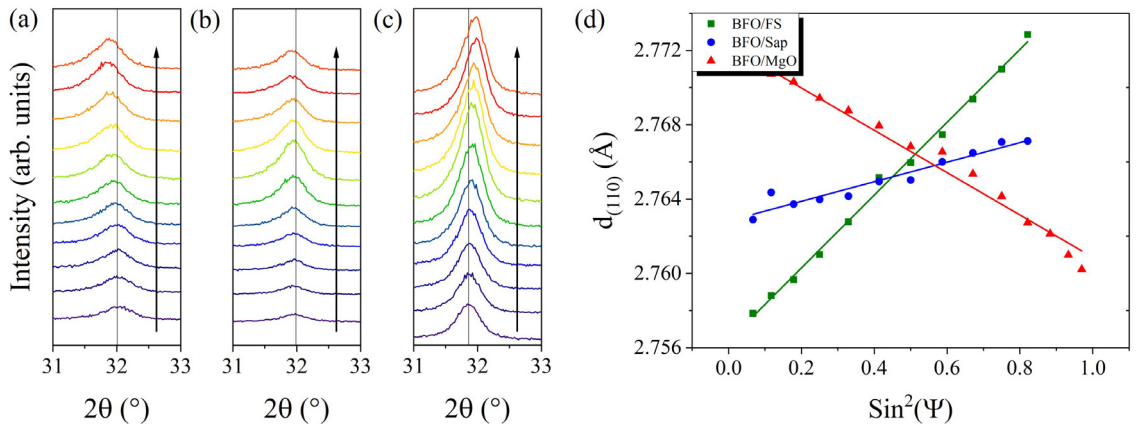

FIG. 2. X-ray pattern of the $(110)_{pc}$ peak as a function of the tilt angle (Ψ) of a polycrystalline BFO film on (a) fused silica, (b) sapphire, and (c) magnesium oxide substrates. The arrow indicates the increase in the tilt angle (Ψ) from 15° to 65°. (d) $d_{(110)}$ vs $\sin^2(\Psi)$ plot.

$$d_\Psi = \frac{1+\nu}{1-\nu}\cdot\varepsilon_{11}\cdot d_0\cdot\sin^2(\Psi) + \left[1-\frac{2\nu}{1-\nu}\cdot\varepsilon_{11}\right]\cdot d_0,$$

where ε_{11} denotes the in-plane strain, $\nu = 0.3$ is the Poisson ratio,[29] and d_0 is the lattice spacing in the absence of stress. Figure 2(d) shows a linear relation between $d_{(110)}$ and $\sin^2(\Psi)$ for all three types of film. The positive slope in BFO/FS and BFO/Sap indicates tensile stress, while the negative slope in BFO/MgO indicates compressive stress. The in-plane strain of the BFO films is 0.38% for BFO/FS, 0.10% for BFO/Sap, and −0.22% for BFO/MgO. Using Young's modulus of 170 GPa of bismuth ferrite,[30] the in-plane tensile stress ($\sigma_{11} = \sigma_{22}$) is calculated as 0.93 GPa for BFO/FS, 0.25 GPa for BFO/Sap, and −0.54 GPa for BFO/MgO. The observation of high tensile stress in the film on fused silica, moderate tensile stress in the film on sapphire, and compressive stress in the film on MgO is in agreement with the qualitative expectations based on the thermal expansion coefficients.

Figure 3(a) compares the polarization hysteresis *P(E)* of BFO/FS, BFO/Sap, and BFO/MgO. The films show a remanent polarization (P_r) of 60 ± 2 μC cm^{-2} for BFO/FS, 56 ± 2 μC cm^{-2} for BFO/Sap, and 53 ± 2 μC cm^{-2} for BFO/MgO and an average coercive field (E_c) of 250 ± 50 kV cm^{-1}. A slight lowering of remanent polarization from the tensile stress to compressive stress is observed. This effect agrees with the expectation for in-plane domain reversal.

Figure 3(b) shows the light ON/light OFF J_{SC} curves of poled BFO/FS, BFO/Sap, and BFO/MgO under 455 nm LED light at an intensity of 0.48 W cm^{-2}. Under illumination, a short-circuit photocurrent (J_{SC}) that depends on the poling direction is generated. The J_{SC} values of the BFO films are 70 ± 2 μA cm^{-2} for BFO/FS, 42 ± 2 μA cm^{-2} for BFO/Sap, and 27 ± 1 μA cm^{-2} for BFO/MgO. An increase in the photocurrent by 150% is, thus, observed from compressive to tensile stress. In Ref. 17, the origin of the photocurrent in BFO/FS was demonstrated to be the BPV effect. This also holds true for the films on the other substrates and is evidenced by the dependence of short-circuit current in the light polarization direction, which can be seen in Fig. S1 of the supplementary material. All samples show a sinusoidal variation of J_{SC} with the angle between light polarization and ferroelectric polarization directions, as is expected for bulk photovoltaic behavior. The relative variation, i.e., the difference between the photovoltaic coefficients β_{311} and β_{333}, is about 8% for BFO/FS and BFO/Sap, but only about 4% for BFO/MgO.

All the films show a similar normalized photoconductivity of 3.3 × 10^{-8} Ω^{-1} W^{-1} cm, 3.2 × 10^{-8} Ω^{-1} W^{-1} cm, and 2.8 × 10^{-8} Ω^{-1} W^{-1} cm for BFO/FS, BFO/Sap, and BFO/MgO, respectively. The *J–V* curves are shown in Fig. S2 of the supplementary material. The sign of the short-circuit photocurrent depends on the poling direction; it is symmetric for both poling directions, an indication that it is not

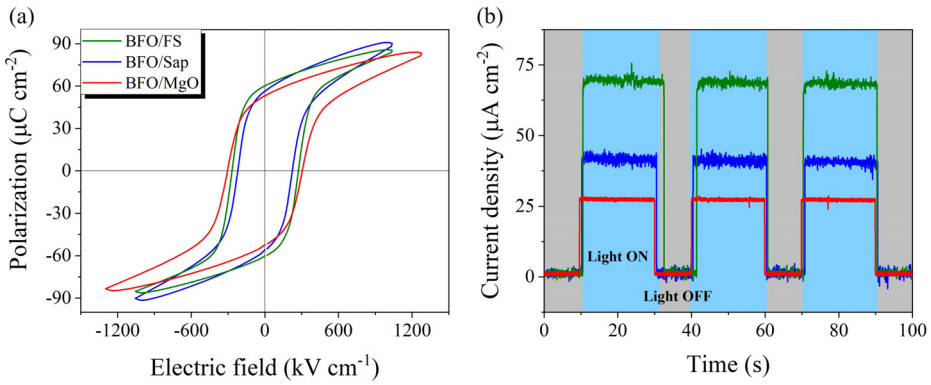

FIG. 3. (a) P(E) loops of BFO deposited on different substrates. (b) ON/OFF J_{SC} values of BFO thin films deposited on different substrates. A 455 nm LED with an intensity of 0.48 W cm^{-2} was used to illuminate the structures.

influenced by extrinsic effects that do not depend on the polarization direction such as potential flexo-photovoltaic contributions[31] arising from a possible strain gradient through the film thickness.

The large increase in the photocurrent cannot be rationalized by the slight increase in the remanent polarization of about 10% between the films under compressive and tensile stress. The microstructure of the three films on the different substrates is also comparable with similar orientation and grain size; therefore, this also cannot account for the changes in the photocurrent. The only major difference between the systems that can account for the different BPV effect, therefore, lies in the degree of stress due to the different thermal expansion coefficient mismatch. It may be argued that this stress might influence light-induced charge transport by generating internal electric fields through the piezoelectric effect. However, with a specific (dark) resistivity of the films around $\rho = 5 \times 10^6\ \Omega$ m,[17] and a permittivity of $\varepsilon = 200$,[24] any such field will be screened by mobile charges with an exponential decay time of $\tau = \rho * \varepsilon * \varepsilon_0 \approx 10^{-2}$ s, i.e., far shorter than the time resolution of our measurements. This explanation can, therefore, be excluded. Two stress-based mechanisms appear plausible to account for the enhancement of the BPV effect in BFO/FS compared to BFO/Sap and BFO/MgO. The first is extrinsic, a stress-induced modification of the domain structure.[2,10–12] The second is intrinsic, a modification of the BPV tensor by the piezophotovoltaic effect.[19,22]

However, the films also show similar domain structures as shown by the PFM characterization of the unpoled films (Fig. S3 of the supplementary material). This agrees with the expectation that a strongly $(100)_{pc}$ oriented film with rhombohedral symmetry should show little domain preference with stress, as all eight domain variants possible in a rhombohedral perovskite are energetically equivalent in this case. In addition, the similar P(E) loops also do not support strongly different domain structures. The presence of comparable domain structures makes the explanation of the different BPV behavior by extrinsic effects unlikely. Instead, the increased photocurrent in BFO/FS is likely a result of an intrinsic piezophotovoltaic effect. The local crystallographic structure is distorted by the stress; tensile stress increases the non-centrosymmetric characteristic, and under tensile stress, the reduced rhombohedral unit cell is distorted toward a higher a(=b)/c lattice parameter ratio, while compressive stress decreases it. This is reflected in the higher remanent polarization in BFO/FS, as shown in Fig. 3(a), where the in-plane projection of the polarization vector is increased. The opposite is observed under compressive stress. This change in asymmetry leads to changes in the photoexcitation of non-thermalized charge carriers, which in turn changes the BPV response.

It must be noted that in contrast to Fe:$LiNbO_3$, where an increase in the BPV current under uniaxial compressive stress was reported,[27] the current increases under biaxial tensile stress in the present case. The exact nature of the piezophotovoltaic effect depends on the physical background of the BPV effect itself. In $LiNbO_3$, it is based on non-thermalized hopping of electrons between polaronic Nb^{4+} sites after excitation from A-site Fe^{2+} defects. In analogy to Fe:$LiNbO_3$, the B-site Mn doping introduces intra-bandgap states[14] that can give rise to a bulk photovoltaic current mechanism similar to Fe:$LiNbO_3$.[32] In that case, a bulk photovoltaic current may be produced by the non-thermalized hopping of electrons from the Mn^{2+} and Mn^{3+} states into a Fe^{2+} state. The change in the sign of β_{31} with and without Mn doping[14] also supports a BPV charge transport dominated by the hoping between Mn^{2+} and Mn^{3+} to Fe^{3+} ions. The excitation probability from Mn^{2+} and Mn^{3+} to the Fe^{3+} surrounding atoms will depend on the interatomic distances. In that case, the enhancement in the photocurrent can be reasonably ascribed to the increased nonthermalized hoping.

Another possible explanation is associated with the shift current mechanism. Rappe *et al.* proposed that the main origin of the bulk photovoltaic effect in $BiFeO_3$ and other ferroelectric perovskites was the shift current mechanism.[33,34] Theoretical calculations have shown that strain can modify the magnitude of this shift current.[22] However, no theoretical calculations of the shift piezophotovoltaic effect can be found on $BiFeO_3$. Whether the origin of the enhancement in the photocurrent is produced by the decrease in the energy of the phonons involved in the non-thermalized hoping or by the enhancement of the shift current is beyond the scope of this work.

In summary, different degrees of stress were applied to polycrystalline bismuth ferrite films by using different substrates. The influence of the in-plane stress on the ferroelectric and BPV properties was measured using IDEs. An increase in the photocurrent of 150% is observed with a change from a compressive stress of −0.54 GPa to a tensile stress of 0.93 GPa. The change in the photocurrent with stress is explained with the intrinsic piezophotovoltaic effect.

The results show that tuning the BPV effect in thin films via the piezophotovoltaic effect is possible. These finding are not only applicable to polycrystalline films but are very promising for highly strained epitaxial films. The combination of high strain, domain structure engineering, and better BPV systems, such as Fe:$LiNbO_3$, could pave the way toward the development of more effective photovoltaic thin films.

See the supplementary material for Figs. S1, S2, and S3.

The authors acknowledge financial support from the Luxembourgish National Research Fund (FNR) under the project PACE (Photovoltaics: Advanced Concepts for high Efficiency, No. PRIDE17/12246511/PACE).

AUTHOR DECLARATIONS

Conflict of Interest

The authors declare that they have no competing interest.

Author Contributions

Alfredo Blázquez Martínez: Methodology (equal); Validation (lead); Formal analysis (lead); Investigation (lead); Resources (equal); Visualization (lead); Writing – original draft (equal); Writing – review & editing (equal). **Patrick Grysan**: Formal analysis (supporting); Investigation (supporting); Visualization (supporting). **Stéphanie Girod**: Resources (supporting). **Veronika Kovacova**: Investigation (supporting); Resources (supporting). **Sebastjan Glinsek**: Supervision (supporting); Writing – review & editing (supporting). **Torsten Granzow**: Conceptualization (lead); Methodology (equal); Supervision (lead); Project administration (lead); Funding acquisition (lead); Writing – original draft (equal); Writing – review & editing (equal).

DATA AVAILABILITY

The data that support the findings of this study are available from the corresponding author upon reasonable request.

REFERENCES

[1]B. I. Sturman and V. M. Fridkin, *The Photovoltaic and Photorefractive Effects in Noncentrosymmetric Materials* (Taylor & Francis Group, 1992).
[2]S. Y. Yang, J. Seidel, S. J. Byrnes, P. Shafer, C.-H. Yang, M. D. Rossell, P. Yu, Y.-H. Chu, J. F. Scott, J. W. Ager, L. W. Martin, and R. Ramesh, Nat. Nanotechnol. **5**, 143 (2010).
[3]J. E. Spanier, V. M. Fridkin, A. M. Rappe, A. R. Akbashev, A. Polemi, Y. Qi, Z. Gu, S. M. Young, C. J. Hawley, D. Imbrenda, G. Xiao, A. L. Bennett-Jackson, and C. L. Johnson, Nat. Photonics **10**, 611 (2016).
[4]R. Guo, L. You, Y. Zhou, Z. Shiuh Lim, X. Zou, L. Chen, R. Ramesh, and J. Wang, Nat. Commun. **4**, 1990 (2013).
[5]S. Köber, M. Salvador, and K. Meerholz, Adv. Mater. **23**, 4725 (2011).
[6]B. Lynn, P.-A. Blanche, and N. Peyghambarian, J. Polym. Sci. Part B Polym. Phys. **52**, 193 (2014).
[7]D. Kip, Appl. Phys. B Lasers Opt. **67**, 131 (1998).
[8]B. Kundys, Appl. Phys. Rev. **2**, 011301 (2015).
[9]C. Chen and Z. Yi, Adv. Funct. Mater. **31**, 2010706 (2021).
[10]H. Matsuo, Y. Kitanaka, R. Inoue, Y. Noguchi, M. Miyayama, T. Kiguchi, and T. J. Konno, Phys. Rev. B **94**, 214111 (2016).
[11]A. Bhatnagar, A. Roy Chaudhuri, Y. Heon Kim, D. Hesse, and M. Alexe, Nat. Commun. **4**, 2835 (2013).
[12]J. Seidel, D. Fu, S.-Y. Yang, E. Alarcón-Lladó, J. Wu, R. Ramesh, and J. W. Ager, Phys. Rev. Lett. **107**, 126805 (2011).
[13]I. Grinberg, D. V. West, M. Torres, G. Gou, D. M. Stein, L. Wu, G. Chen, E. M. Gallo, A. R. Akbashev, P. K. Davies, J. E. Spanier, and A. M. Rappe, Nature **503**, 509 (2013).
[14]H. Matsuo, Y. Noguchi, and M. Miyayama, Nat. Commun. **8**, 207 (2017).
[15]H. Mai, T. Lu, Q. Sun, J. Langley, N. Cox, F. Kremer, T. Duong, K. Catchpole, H. Chen, Z. Yi, T. J. Frankcombe, and Y. Liu, J. Mater. Chem. A **9**, 13182 (2021).
[16]M. M. Yang and M. Alexe, Adv. Mater. **30**, 1704908 (2018).
[17]A. Blázquez Martínez, P. Grysan, S. Girod, S. Glinsek, and T. Granzow, Scr. Mater. **211**, 114498 (2022).
[18]M.-M. Yang, D. J. Kim, and M. Alexe, Science **360**, 904 (2018).
[19]S. Nadupalli, J. Kreisel, and T. Granzow, Sci. Adv. **5**, eaau9199 (2019).
[20]N. Aruchamy, T. Schenk, S. Girod, S. Glinsek, E. Defay, and T. Granzow, J. Appl. Phys. **131**, 014101 (2022).
[21]G. L. Brennecka, W. Huebner, B. A. Tuttle, and P. G. Clem, J. Am. Ceram. Soc. **87**, 1459 (2004).
[22]A. M. Schankler, L. Gao, and A. M. Rappe, J. Phys. Chem. Lett. **12**, 1244 (2021).
[23]C. Guo-Feng, R. Yin-Jie, S. Yue, and Y. Han-Di, J. Inorg. Mater. **34**, 1128–1133 (2019).
[24]A. Blázquez Martínez, N. Godard, N. Aruchamy, C. Milesi-Brault, O. Condurache, A. Bencan, S. Glinsek, and T. Granzow, J. Eur. Ceram. Soc. **41**, 6449 (2021).
[25]X. Zheng, J. Li, and Y. Zhou, Acta Mater. **52**, 3313 (2004).
[26]T. Schenk, C. M. Fancher, M. H. Park, C. Richter, C. Künneth, A. Kersch, J. L. Jones, T. Mikolajick, and U. Schroeder, Adv. Electron. Mater. **5**, 1900303 (2019).
[27]W. Kang, Y. Li, Z. Zheng, S. Yan, and R. Zhao, J. Mater. Sci. Mater. Electron. **31**, 5746 (2020).
[28]A. Kumar and D. Varshney, Ceram. Int. **38**, 3935 (2012).
[29]S. Hu, A. Alsubaie, Y. Wang, J. H. Lee, K.-R. Kang, C.-H. Yang, and J. Seidel, Phys. Status Solidi **214**, 1600356 (2017).
[30]S.-R. Jian, H.-W. Chang, Y.-C. Tseng, P.-H. Chen, and J.-Y. Juang, Nanoscale Res. Lett. **8**, 297 (2013).
[31]R. Guo, L. You, W. Lin, A. Abdelsamie, X. Shu, G. Zhou, S. Chen, L. Liu, X. Yan, J. Wang, and J. Chen, Nat. Commun. **11**, 2571 (2020).
[32]O. F. Schirmer, M. Imlau, and C. Merschjann, Phys. Rev. B - Condens. Matter Mater. Phys. **83**, 165106 (2011).
[33]S. M. Young, F. Zheng, and A. M. Rappe, Phys. Rev. Lett. **109**, 236601 (2012).
[34]S. M. Young and A. M. Rappe, Phys. Rev. Lett. **109**, 116601 (2012).